AUTHOR QUERY FORM

ELSEVIER	**Journal:** WEA **Article Number:** 99736	**Please e-mail or fax your responses and any corrections to:** **E-mail:** corrections.esch@elsevier.thomsondigital.com **Fax:** +353 6170 9272

Dear Author,

Please check your proof carefully and mark all corrections at the appropriate place in the proof (e.g., by using on-screen annotation in the PDF file) or compile them in a separate list. To ensure fast publication of your paper please return your corrections within 48 hours.

For correction or revision of any artwork, please consult http://www.elsevier.com/artworkinstructions.

Any queries or remarks that have arisen during the processing of your manuscript are listed below and highlighted by flags in the proof. Click on the 'Q' link to go to the location in the proof.

Location in article	Query / Remark: click on the Q link to go Please insert your reply or correction at the corresponding line in the proof
Q1	Please provide an update for reference [23], in press.

Thank you for your assistance.

Wear xxx (2011) xxx–xxx

Contents lists available at ScienceDirect

Wear

journal homepage: www.elsevier.com/locate/wear

Microstructural characterization and tribocorrosion behaviour of Al/Al_3Ti and Al/Al_3Zr FGMs

S.C. Ferreira [a], P.D. Sequeira [a], Yoshimi Watanabe [b], E. Ariza [a], L.A. Rocha [a,*]

[a] Centre for Mechanical and Materials Technologies, Department of Mechanical Engineering, University of Minho, Campus de Azurém, 4800-058 Guimarães, Portugal
[b] Department of Engineering Physics, Electronics and Mechanics, Graduate School of Engineering, Nagoya Institute of Technology, Gokiso-Chu, Showa-Ku, 466-8555 Nagoya, Japan

ARTICLE INFO

Article history:
Received 30 March 2010
Received in revised form 12 February 2011
Accepted 16 February 2011
Available online xxx

Keywords:
Metal–matrix composites (MMCs)
Functional composites
Corrosion
Tribocorrosion
Casting

ABSTRACT

Al/Al_3Ti and Al/Al_3Zr functionally graded materials (FGMs) were manufactured through a centrifugal method from Al–5 mass % Ti and Al–5 mass % Zr, respectively. Applied centrifugal forces were 30, 60 and 120 *G* (units of gravity). Microstructural characterization was performed and the influence of the reinforcing phase on the tribocorrosion behaviour of the FGMs was investigated. An increase in both the particles volume fraction as well as their orientation in the outer regions of the FGMs was found as the applied centrifugal force increased. Better tribocorrosion behaviour was found in the samples containing the highest concentration of reinforcing particles. However the microstructure below the surface appears to influence the tribocorrosion behaviour.

1. Introduction

Dispersion of hard intermetallic compounds in Al alloys has been studied as a means to improve the alloys' mechanical properties [1–4]. When the reinforcing phase has a higher density than the matrix, the centrifugal method is attractive due to the fact that there is a selective reinforcement of the surface of the component while gradually increasing the relative amount of ductile phases towards the inner region [5–8]. This results in a higher wear resistance in the surface as well as maintaining high bulk toughness. In fact, the presence of the reinforcing phase, in this case Al_3Ti or Al_3Zr platelets, has a strong influence on the local mechanical properties. The shape, size and spatial orientation of the reinforcing phase will also play an essential role on the wear performance of the material [9,10].

As stated above, particle segregation during casting with the centrifugal method occurs due to the difference in density between the particles and molten alloy [11]. Therefore, the study of two Al/intermetallic compounds systems where the intermetallic compounds have different density values, Al_3Ti and Al_3Zr have densities of 3.4 and 4.1 g cm^{-3}, respectively, is of interest.

There are some published works dealing, independently, on the wear or corrosion behaviour of composites reinforced with intermetallic particles. However, no studies were published on the tribocorrosion behaviour of this kind of materials when they are in contact with aggressive environments. The tribocorrosion behaviour of the Al/Al_3Ti and Al/Al_3Zr FGMs is important to evaluate, since particulate reinforced Al matrix composites (AlMCp) have received increasing demands for aerospace and automotive applications [12]. Compared to ceramic reinforcements, the employment of intermetallics as mechanical resistant reinforcements has advantages. In addition to their high level of hardness, elastic modulus, melting temperature and thermal stability, the thermal expansion coefficients of intermetallics is much closer to those of Al alloys. The smaller discrepancy in thermal expansion coefficients will decrease the residual stress at reinforcement/matrix interfaces when the composite is exposed to thermal cycles, hence guarantying a lower degree of failure originated at the interface [13].

The material exposed to a tribocorrosion environment, i.e., where interactions between mechanical and corrosion degradation processes occur, suffers an irreversible transformation which can lead to the decrease of its performance [14]. The total metal removal rate is usually not simply the sum of the corrosion rate and the wear rate measured in separate experiments. In many cases corrosion is accelerated by wear and, similarly, wear may be accelerated by corrosion [15]. The mutual dependence of mechanical and chemical metal removal rates in a tribocorrosion system can be due to phenomena such as: local abrasion of the passive film leading to wear accelerated corrosion due to rapid dissolution of the locally

* Corresponding author. Tel.: +351 253 510220; fax: +351 253 516007.
E-mail address: lrocha@dem.uminho.pt (L.A. Rocha).

0043-1648/$ – see front matter © 2011 Published by Elsevier B.V.
doi:10.1016/j.wear.2011.02.007

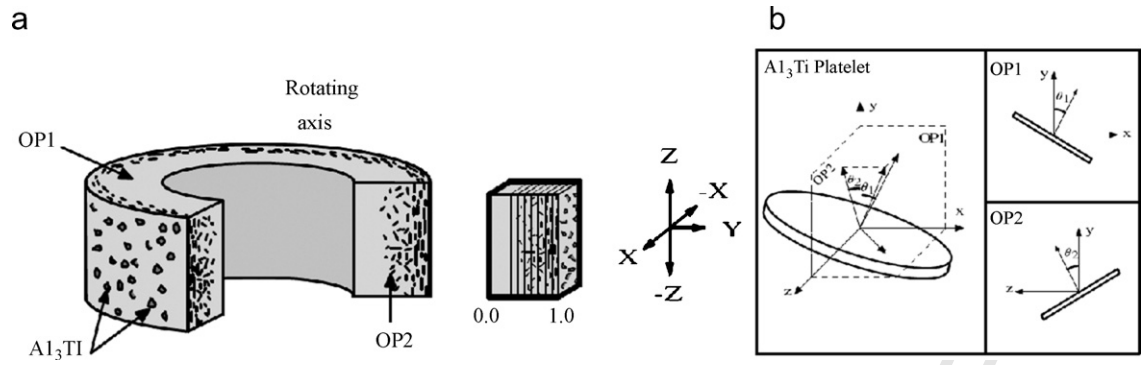

Fig. 1. (a) Schematic representation of the FGM ring. (b) Definition of orientation angle, θ.

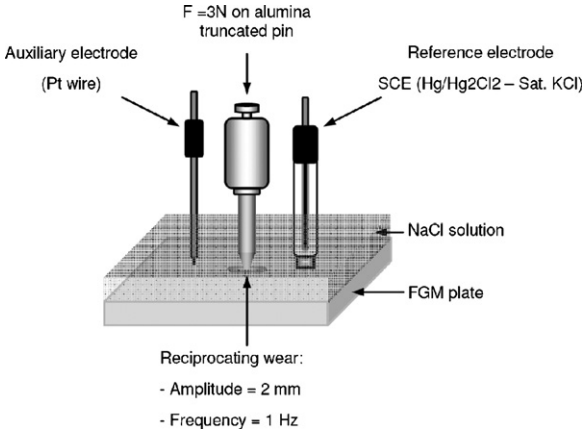

Fig. 2. Schematic view of the tribocorrosion test setup.

depassivated metal surface, followed by repassivation; the abrasive action of hard oxide particles formed by corrosion which will accelerate the mechanical metal removal by wear; the plastic deformation of the surface layer of a rubbing metal leading to transfer of material to the opposite body resulting in a reduction of corrosion, and others [14–16].

In the present study microstructural characterization was performed on Al/Al_3Ti and Al/Al_3Zr FGMs processed with different applied centrifugal forces. Also tribocorrosion behaviour of Al/Al_3Ti and Al/Al_3Zr FGMs has been studied in the outer region of the FGM rings.

Table 1
Crystal structure and density.

Element or compound	Crystal structure	Density ($g\,cm^{-3}$)
Al	*Fcc*	2.7
Al_3Ti	$D0_{22}$	3.3
Al_3Zr	$D0_{23}$	4.1

2. Material and methods

Al/Al_3Ti and Al/Al_3Zr FGMs were produced by the centrifugal method, from Al–5 mass % Ti and Al–5 mass % Zr commercial alloys, respectively. The crystal structures and densities of the intermetallic compounds and those of Al are presented in Table 1. Since the

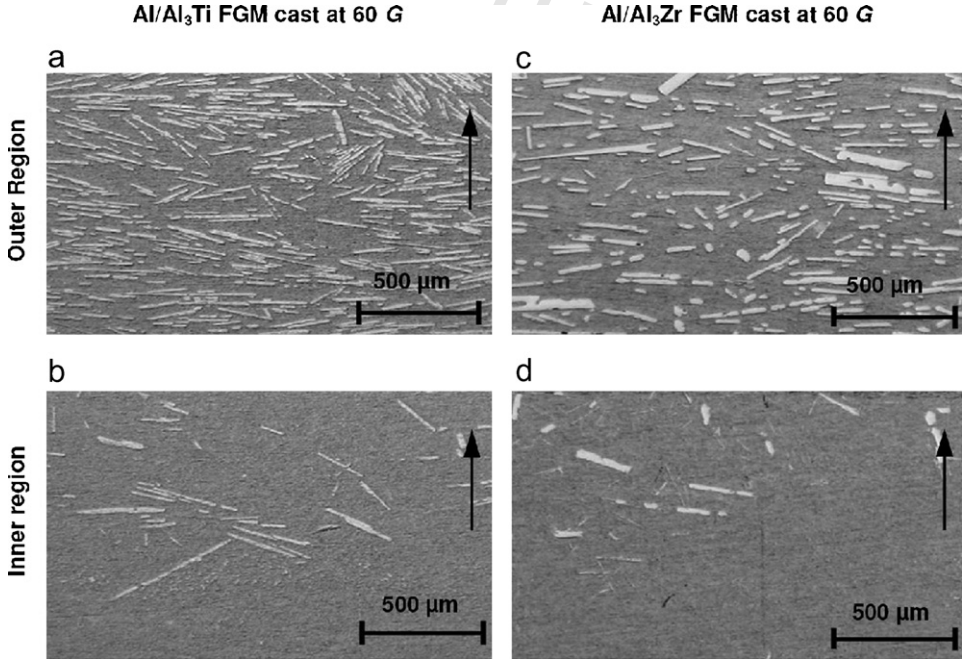

Fig. 3. Optical micrographs, brighter areas are the intermetallic particles. (a) and (b) are from the Al/Al_3Ti FGM cast at 60 *G* at the outer and interior regions, respectively. (c) and (d) are from the Al/Al_3Zr FGM cast at 60 *G* at the outer and interior regions, respectively. The arrows indicate the direction of applied centrifugal force.

Please cite this article in press as: S.C. Ferreira, et al., Microstructural characterization and tribocorrosion behaviour of Al/Al_3Ti and Al/Al_3Zr FGMs, Wear (2011), doi:10.1016/j.wear.2011.02.007

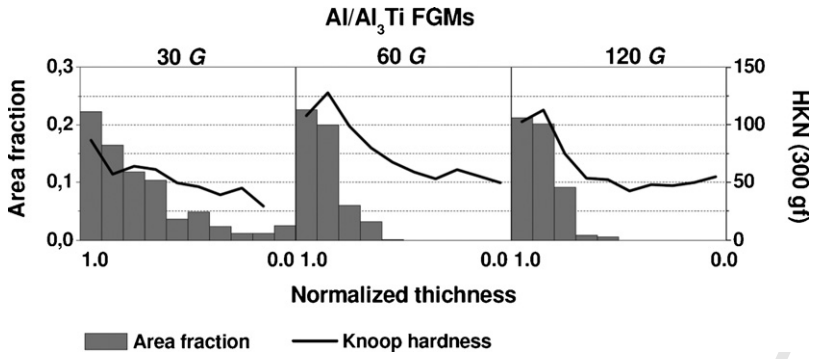

Fig. 4. Intermetallic particles area fraction and knoop hardness evolution for the Al/Al_3Ti FGMs.

relative atomic masses of Al, Ti and Zr are 26.98, 47.88 and 91.22, respectively, the theoretical volume fraction of Al_3Ti in the master alloy was calculated to be approximately 11 vol% and that of Al_3Zr as approximately 7 vol%.

In the centrifugal method the alloy was heated up to a temperature located between its *solidus* and *liquidus* temperatures, were most of the intermetallic platelets remain solid in a liquid Al-based matrix. It was then poured into a rotating mould in order to obtain ring-shaped samples which have an outer diameter of 90 mm, 25 mm in height and a length of 20–25 mm. The temperature of the melting furnace was 1173 K and the applied centrifugal casting forces were 30, 60 and 120 *G* (units of gravity). A detailed description of the centrifugal method is available elsewhere [5–9].

Samples were cut, polished and divided into ten regions of equal width along the centrifugal force direction. The outer surface of the ring is represented as the position 1.0 of the normalized distance and the inner surface by the position 0.0.

Optical micrographs were taken and from those intermetallic particles distribution, size, shape and orientation were measured along two planes, perpendicular to the rotating axis (referred as OP1) and perpendicular to the rotating direction (referred as OP2), as seen in Fig. 1. Knoop hardness tests were performed, with the indenter's long diameter normal to the centrifugal force direction.

Potentiodynamic polarisation curves of both Al/Al_3Ti and Al/Al_3Zr FGMs samples were obtained in a 0.6 M NaCl solution by scanning the potential from −1.4 to 0.2 V at a scan rate of 2 mV s^{-1} using a PGP201 Potentiostat/Galvanostat (Radiometer Denmark), controlled by the VoltaMaster-1 software. The area of the working electrode was set in 0.4 cm^2, the counter electrode was a Pt wire with an area of 1 cm^2 and a saturated calomel electrode (SCE) was used as reference.

Tribocorrosion behaviour was studied in the outer region of the Al/Al_3Ti and Al/Al_3Zr FGMs in the plane perpendicular to the axis of rotation of the rings. These tests were performed using a reciprocating tribometer (Plint TE67/R). An alumina (Al_2O_3) pin (truncated cone geometry and with a tip of 1 mm in diameter) was used as counter-body and mounted vertically on the samples immersed in the electrolyte (exposed area = 0.95 cm^2). The samples were used as plates positioned horizontally and mounted in an acrylic electrochemical cell (20 ml of a 0.6 M NaCl solution was used as electrolyte), as seen in Fig. 2. All potentials were measured and expressed with reference to a standard calomel electrode (SCE), and a Pt wire with an area of 1 cm^2 served as counter electrode. A Voltalab PGZ100 Potentiostat (Radiometer Analytical, Denmark), controlled by Voltamaster-4 software was used in the electrochemical measurements. Samples were previously cathodically polarised at −1.4 V vs. SCE, during 3 min, in order to clean the surface. Then, a potential of −0.83 V vs. SCE was applied and kept during the subsequent steps (potentiostatic control). This potential was selected from the potentiodynamic polarisation curves and lies in the active zone, near the corrosion potential of the samples. After, the mechanical contact between the alumina pin and the sample plate was established. The reciprocating wear test was performed with a normal load of 3 N, displacement amplitude of 2 mm and a frequency of 1 Hz. The sliding time was 900 s. When sliding was stopped, the pin and the sample were removed from the solution and ultrasonically cleaned in ethanol and dried. For each sample, the tests were repeated twice. The total wear volume, caused by the contribution of wear and corrosion, was determined by the profilometric method, using a Perthometer S5P roughness meter, by calculating the average of the cross-sectional area multiplied by the stroke length. The chemical wear volume (V_{chem}) was determined from the measured electrical charge, using Faraday's law:

$$V_{chem} = \frac{Q \bullet M}{n \bullet F \bullet \rho} \quad (1)$$

where, Q is the electric charge, which is obtained by integrating of the current density curve with the time, along of the sliding

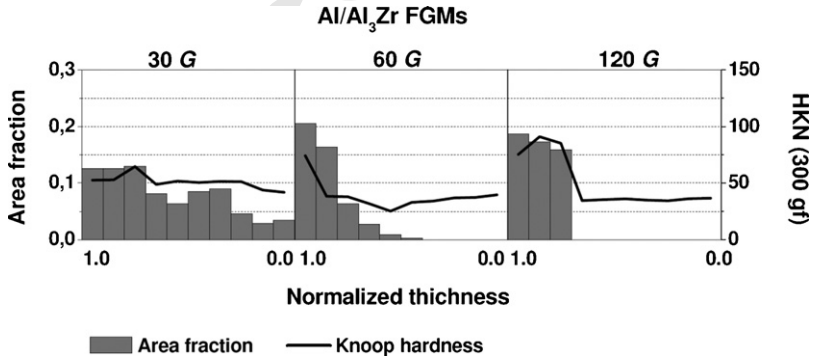

Fig. 5. Intermetallic particles area fraction and knoop hardness evolution for the Al/Al_3Zr FGMs.

Please cite this article in press as: S.C. Ferreira, et al., Microstructural characterization and tribocorrosion behaviour of Al/Al_3Ti and Al/Al_3Zr FGMs, Wear (2011), doi:10.1016/j.wear.2011.02.007

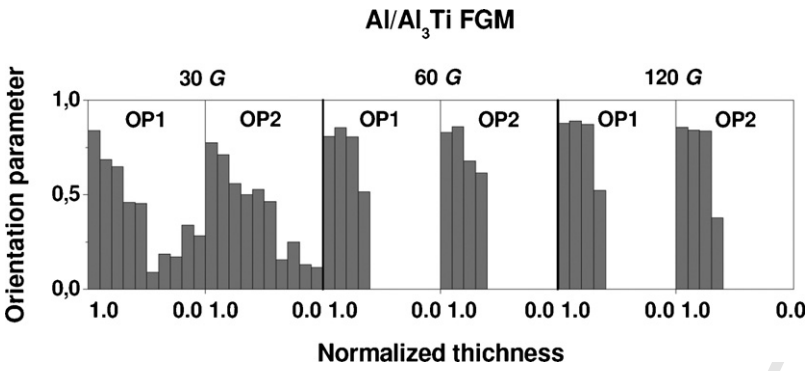

Fig. 6. Al_3Ti platelets Hermans orientation parameter distribution.

time ($Q = \int I\,dt$), M is the atomic mass of aluminium ($27\,g\,mol^{-1}$), n the valence of dissolution of the Al (+3), F the Faraday's constant ($9.649 \times 10^{-4}\,C\,mol^{-1}$) and ρ is the density of the Al ($2.7 \times 10^{-3}\,g\,mm^{-3}$). The mechanical wear volume, which is the volume of material removed mechanically, was obtained by subtraction of the calculated chemical wear volume to the total wear volume.

The topographical features of the worn surfaces were investigated using scanning electron microscopy (SEM) in an attempt to study the tribocorrosion mechanisms.

3. Results and discussion

3.1. Intermetallic compounds volume fraction and knoop hardness distributions

Optical micrographs of the typical microstructure found in the produced FGMs are shown in Fig. 3. The volume fraction of Al_3Ti in the Al/Al_3Ti FGM and that of Al_3Zr in the Al/Al_3Zr FGM as a function of normalized distance are seen in Figs. 4 and 5, respectively. It is observed from Figs. 4 and 5 that in all samples the volume fraction occupied by Al_3Ti or Al_3Zr particles decreases from the outer (1.0 position in the abscissa of the figures) to the inner regions (position 0.0) of the FGM rings. In fact, with samples cast under 60 and 120 G there is an absence of particles from around the middle to the inner region of the rings in both the Al/Al_3Ti and Al/Al_3Zr FGMs.

As seen in Fig. 4, an increase in the applied centrifugal force does not appear to significantly increase the intermetallic particle fraction at the outermost region of the Al/Al_3Ti FGMs rings, which remain around 20–25 vol%, but does increase the volume fraction in the adjacent regions. As expected, due to the initial lower theoretical volume fraction, all the Al/Al_3Zr FGMs present lower volume fractions than the Al/Al_3Ti FGMs (see Fig. 5).

At applied centrifugal force of 30 G the Al/Al_3Zr FGM exhibits a very low gradient when compared to the Al/Al_3Ti sample. The samples from both systems cast at 60 G display a very similar trend while, for the samples subjected to a centrifugal force of 120 G, a higher relative clustering of particles on the outermost regions is found for the Al/Al_3Zr FGM. Al_3Ti particles have a higher segregation rate with lower applied centrifugal forces than the Al_3Zr particles; a situation that is reversed for higher applied centrifugal forces.

It has been accepted, in general, that the viscosity of a suspension rises with to the increase in number of particles in the suspension [17]. Since the motion of spherical particles in a viscous liquid under a centrifugal force can be determined by the simple Stokes' law, the volume fraction gradient within the spherical particle reinforced FGM becomes steeper by decreasing the mean volume fraction of particles [7]. Easier migration of the particles in sparser suspensions, compared with denser suspensions, could not explain the lower gradient obtained in the Al/Al_3Zr FGMs at low applied centrifugal force when compared to the Al/Al_3Ti FGMs. In this way, the present results, relating to the effect of mean volume fraction, contradicts the previous results for spherical particles [7]. On the other hand the same effect has been found to occur in Al/Al_3Ti FGMs with different volume fraction of particles, that is, an increase in volume fraction leads to steeper gradients [18]. Therefore it is apparent that the simple Stokes' law is not applicable to the Al/Al_3Ti and Al/Al_3Zr systems.

Knoop hardness measurements for the Al/Al_3Ti FGMs (Fig. 4) in general follow the same trend as the area fraction for each sample, with values around 50 HKN in the regions without particles and over 100 in areas with the higher intermetallic content. A similar trend, although with slightly lower values of maximum hardness, is also observed in the Al/Al_3Zr FGMs (Fig. 5). The Al_3Ti and Al_3Zr intermetallic compounds show Vickers hardness of the same order of magnitude: 4–7 GPa for Al_3Ti and 4.27–7.4 GPa for Al_3Zr [19].

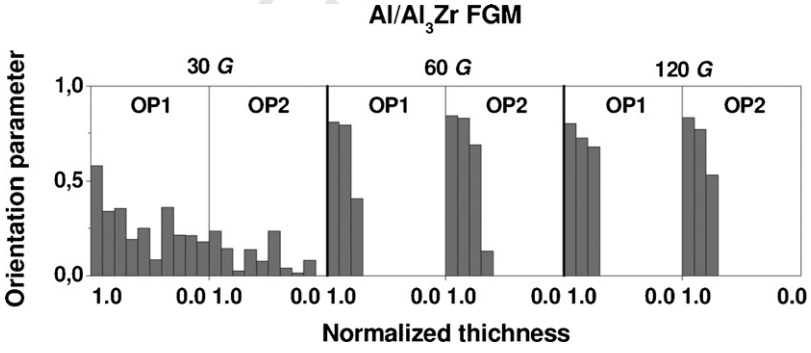

Fig. 7. Al_3Zr platelets Hermans orientation parameter distribution.

Please cite this article in press as: S.C. Ferreira, et al., Microstructural characterization and tribocorrosion behaviour of Al/Al_3Ti and Al/Al_3Zr FGMs, Wear (2011), doi:10.1016/j.wear.2011.02.007

However, the Al/Al_3Ti FGMs show higher hardness in the outermost regions as a consequence of a higher concentration of intermetallic particles when compared to the Al/Al_3Zr FGMs.

3.2. Orientation distribution of Al_3Zr and Al_3Ti platelets

As mentioned above, it was found that in the outer region of the ring, most of platelets are oriented with their planes nearly perpendicular to the radial direction (see Fig. 3). In order to describe the degree of orientation, it is necessary to define the reference axes, *x*, *y* and *z*, as shown in Fig. 1. Planes OP1 and OP2 correspond to *x*–*y* plane and *y*–*z* plane, respectively. Fig. 1b) shows the definition of the orientation angles θ_1 and θ_2 on the planes OP1 and OP2, respectively. Two-dimensional (2-D) orientation of the platelet can be described by the angle, θ, between the direction perpendicular to the disc plane and the reference axis, *y* (the centrifugal force direction, i.e. radial direction of the ring as shown in Fig. 1a). The 2-D platelet orientation distributions are obtained from micrographs. Furthermore, in order to quantitatively describe this orientation tendency quantitatively, the following Hermans orientation parameter, *fp* [20–22] was calculated.

$$fp = [2\langle\cos^2\theta\rangle - 1] \quad (2)$$

Where the trigonometric average is,

$$\langle\cos^2\theta\rangle = \int_{-\pi/2}^{\pi/2} \cos^2\theta\, n(\theta)\, d\theta \quad (3)$$

The term $n(\theta)$ is the orientation distribution function which specifies the fraction of platelets within the angular element $d\theta$. The parameter *fp* becomes 0 for a random distribution of platelets, and it becomes 1 for perfect alignments of the platelets with their planes perpendicular to the direction of the applied centrifugal force. Intermediate values of this parameter correspond to partial states of orientation.

As seen in Figs. 6 and 7 the platelets tend to be oriented normal to the centrifugal force direction. The trend is similar along both observation planes (OP1 and OP2) in agreement with previous studies [17,22], with exception of the Al/Al_3Zr sample cast under 30 *G*. Also the orientation of platelets in the outer regions is increased with the increase in applied centrifugal force, although, as with the volume fraction values, the increase of applied centrifugal force from 60 to 120 *G* does not affect significantly the orientation parameter for the outermost region but does increase it for the adjacent regions, a similar effect is observed for the Al/Al_3Zr FGMs. Also higher orientation parameter values are obtained for the Al/Al_3Ti FGMs. The higher volume fraction of Al_3Ti platelets leads to the necessity of a closer packing between them, which is facilitated by their shape and size (see Fig. 3). As for the behaviour of the Al_3Zr platelets, a very low orientation parameter is found in the outer regions of the sample cast under 30 *G* and an essentially random orientation in the interior regions. The low particle orientation in this sample is furthermore corroborated by the lack of correlation between the observed values in OP1 and OP2. At applied centrifugal forces of 60 and 120 *G*, the Al/Al_3Zr FGMs follow the same trend as the Al/Al_3Ti FGMs although with a lower overall value, in this case the lower volume fraction allows for a greater freedom of movement of the Al_3Zr platelets, leading to lower orientation parameter values.

3.3. Tribocorrosion behaviour

Before the tribocorrosion tests, potentiodynamic polarisation curves were performed with the aim of selecting the potential applied in the tribocorrosion tests. Potentiodynamic polarisation curves obtained in all samples are shown in Fig. 8. As can be

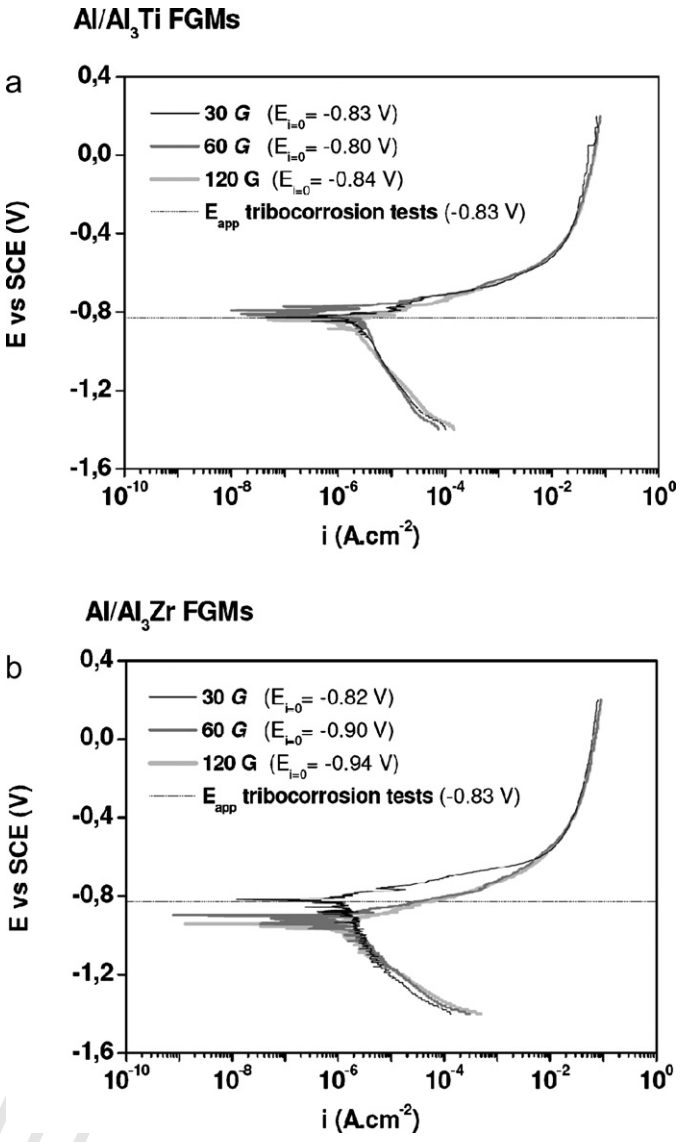

Fig. 8. Representative potentiodynamic polarisation curves obtained in the FGMs immersed in a 0.6 M NaCl solution: (a) Al/Al_3Ti FGMs and (b) Al/Al_3Zr FGMs.

observed in Fig. 8a), the corrosion potential ($E_{i=0}$) values of Al/Al_3Ti 30, 60 and 120 *G* samples are very similar, −0.83, −0.80 and −0.84 V, respectively. In the case of the Al/Al_3Zr FGMs (Fig. 8b), the samples present a more dispersed behaviour. The 30 *G* sample reveals a corrosion potential ($E_{i=0}$) of −0.83 V clearly higher than the 60 *G* and 120 *G* samples, −0.90 and −0.94 V, respectively. The determination of the corrosion current density (i_{corr}) for all samples presents some difficulties because of the high noise level and instability of the samples immersed in the electrolyte. As a result, the potential of −0.83 V vs. SCE was selected to perform the tribocorrosion test, which was performed at potentiostatic control. As can be seen in Fig. 8, this value is close of the active zone, relatively close to the corrosion potential of the samples.

Results of the tribocorrosion tests obtained in Al/Al_3Ti FGMs samples are presented in Fig. 9, which shows the evolution of the current density (i) and of the friction coefficient (μ), with the time. All samples show an increase in the current density at the beginning of sliding, corresponding to the exposure of fresh active material that becomes in contact with the solution. Nevertheless, after some time of sliding, the current density decreases until reaching the steady-state. The 30 and 120 *G* sample achieves a steady-state after

Please cite this article in press as: S.C. Ferreira, et al., Microstructural characterization and tribocorrosion behaviour of Al/Al_3Ti and Al/Al_3Zr FGMs, Wear (2011), doi:10.1016/j.wear.2011.02.007

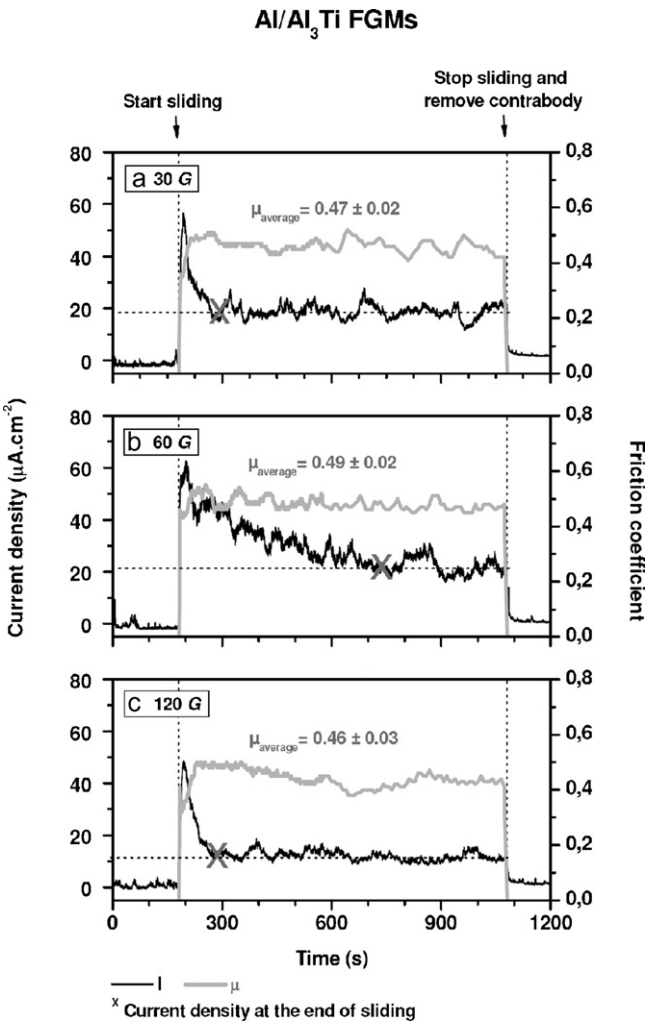

Fig. 9. Evolution of the current and the friction coefficient with time for the Al/Al_3Ti FGMs: (a) 30 *G*, (b) 60 *G* and (c) 120 *G*.

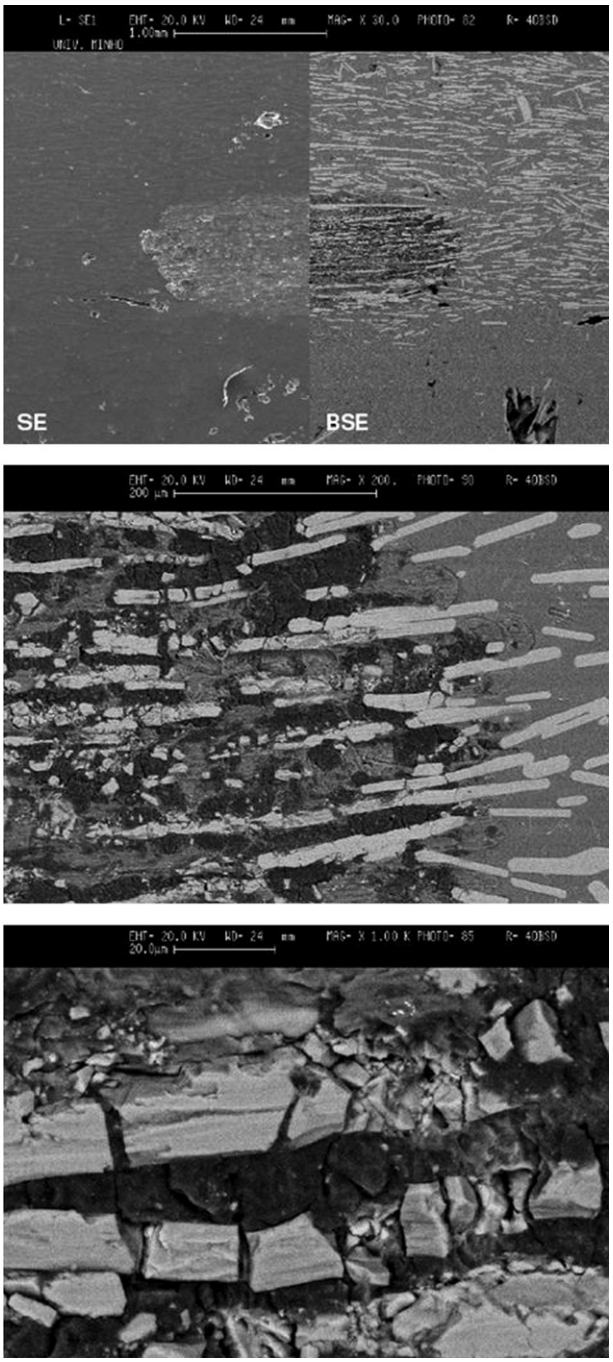

Fig. 10. SEM micrograph revealing the detailed topographical features from surface of Al/Al_3Ti FGM 120 *G* after sliding against an alumina pin in 0.6 M NaCl: (a) wear scar, (b) interface between worn and unworn regions and (c) detail of the Al_3Ti platelets fragments at the wear track.

~100 s of the beginning of the sliding, while the 60 *G* sample takes much more time to reach a steady-state. It is possible to observe that at the end of sliding the 30 and 60 *G* samples have similar current values (~20 μA cm^{-2}, as indicated in Fig. 9). An exception occurs with the 120 *G* sample, which presents the lowest current (~10 μA cm^{-2}). In terms of friction coefficient, μ, all samples show values between 0.4 and 0.6. The average friction coefficient was calculated eliminating the initial sliding values, i.e., by ignoring the running-in period and the lowest value of $\mu_{average}$ corresponded to the 120 *G* sample. Thus, although all samples show similar behaviour, this last sample (120 *G*) presents a relatively better tribocorrosion behaviour when compared with the other samples, by considering the relative lower friction coefficient and current density.

Fig. 10(a) presents the overall topography of Al/Al_3Ti FGM 120 *G* wear track, in which some of the pores arising from the cast process can be observed in the unworn surface. As it can be observed in Fig. 10(b), in which the interface between the wear track and the unworn surface is shown, the Al_3Ti platelets are fractured due to the mechanical action. Nevertheless, around the platelets accumulation of wear debris in the form of a tribolayer can be observed, indicating that the platelets are anchoring that tribolayer around them. In previous works regarding Al-based functionally graded materials reinforced with SiC particles [23,24], it could be observed that the reinforcing particles tend to act as load-bearing elements, promoting the formation and stability of adherent thick tribolayers, improving the wear resistance of the composite. Also, in Al-alloy/SiC composites, the wear rate of the Al-alloy matrix depends on the formation rate of the adherent tribolayer. If the rate of formation of the tribolayer is high, the Al matrix will become protected and its degradation by wear will decrease. In the case of the present study, as shown in Fig. 10(c), the integrity of the Al_3Ti platelets is destroyed due to the mechanical action, being fractured into smaller fragments. However, these fragments remain at the contact region, and are able, of offering some anchoring regions for the tribolayers.

Please cite this article in press as: S.C. Ferreira, et al., Microstructural characterization and tribocorrosion behaviour of Al/Al_3Ti and Al/Al_3Zr FGMs, Wear (2011), doi:10.1016/j.wear.2011.02.007

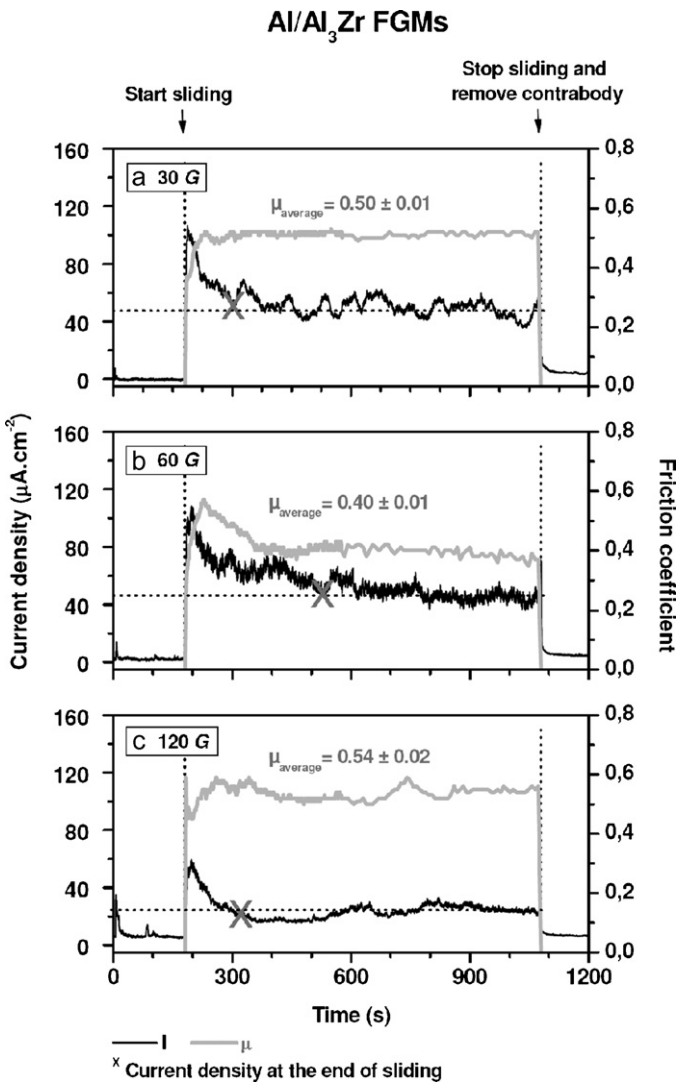

Fig. 11. Evolution of the current and the friction coefficient with time for the Al/Al_3Zr FGMs: (a) 30 *G*, (b) 60 *G* and (c) 120 *G*.

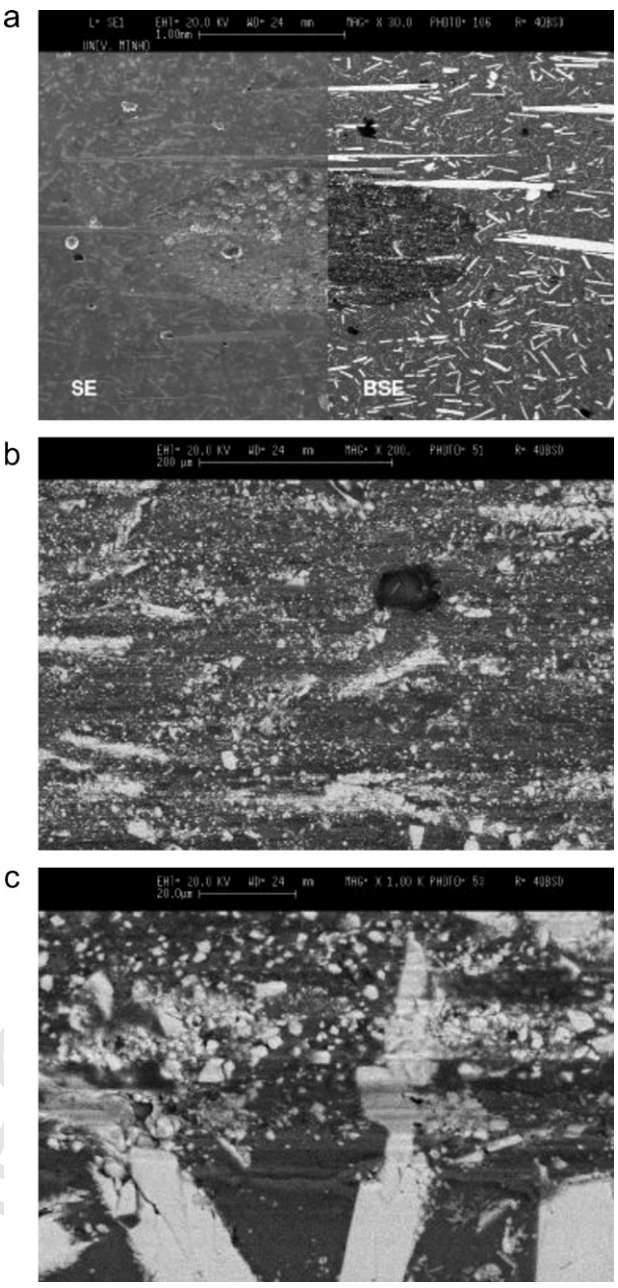

Fig. 12. SEM micrograph revealing the detailed topographical features from surface of Al/Al_3Zr FGM 120 G after sliding against an alumina pin in 0.6 M NaCl: (a) wear scar, (b) detail of the inside of the wear track and (c) detail of the interface between worn and unworn regions.

In Fig. 11, the evolution of current density (i) and of friction coefficient (μ) with the time is presented for the Al/Al_3Zr FGM samples. The 30 and 60 *G* samples show similar current values through the sliding period (~50 μA cm^{-2}), which is very high when compared with the 120 *G* sample (~20 μA cm^{-2}). Friction coefficient, in all samples, varies between 0.4 and 0.6. The sample with the more stable μ during the sliding period is the 30 *G* sample, with a μ of approximately of 0.5. The sample with the lowest μ (~0.4 at the end of sliding) is the 60 *G* sample; in this sample the μ after reaching a maximum value (approximately 0.6) decreases rapidly and stabilizes. In the case of the 120 *G* sample, the friction coefficient is more unstable throughout the sliding time and is the highest (~0.54) when compared with the other samples. Fig. 12(a) shows the overall topography of Al/Al_3Zr FGM 120 *G*. As evidenced in Fig. 12(b) and (c) in this case the platelets were pulverized and crushed in the contact region during sliding against the alumina counter-body. There was no evidence of the formation of a tribolayer, and very thin plowing grooves oriented parallel to the sliding motion can be observed.

In general terms, it can be concluded that the Al/Al_3Zr FGMs samples have worse tribocorrosion behaviour when compared with the Al/Al_3Ti FGMs samples. This assumption is made on the basis of high friction coefficient, higher current density values and on the morphology of the wear scar.

Normally, in tribocorrosion systems an increase in current is observed at the start of sliding, indicating an increase in corrosion rate, also, in passive materials, the passive film is periodically removed by abrasion followed by metal oxidation until repassivation occurs. Also, mechanical wear results on the detachment of particles during sliding which has influence in the coefficient of friction [25]. In the case of the Al/Al_3Ti and Al/Al_3Zr FGMs, the repassivation is expected to be dependent of the galvanic current between matrix and platelets. In fact, Al_3Ti and Al_3Zr show a more noblest potential than the pure Al (pure $Al_{[99,99\%]}$ = −849 mV_{SCE}; Al_3Ti = −799 mV_{SCE} and Al_3Zr = −801 mV_{SCE} in 0.6 M NaCl solution) [26]. The Al/Al_3Ti FGMs samples show lower current densities dur-

Please cite this article in press as: S.C. Ferreira, et al., Microstructural characterization and tribocorrosion behaviour of Al/Al_3Ti and Al/Al_3Zr FGMs, Wear (2011), doi:10.1016/j.wear.2011.02.007

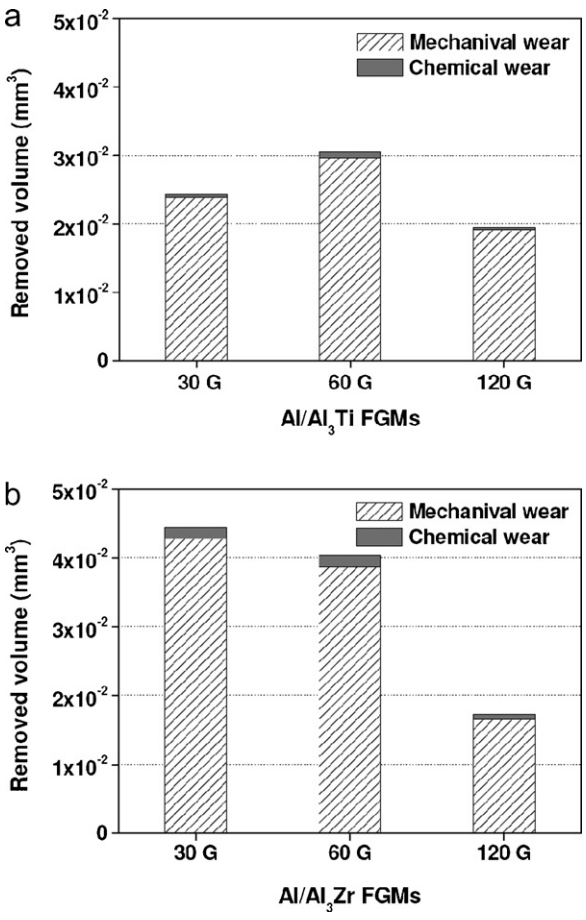

Fig. 13. Removed volumes by mechanical and electrochemical processes, in the tribocorrosion tests: (a) Al/Al_3Ti FGMs samples and (b) Al/Al_3Zr FGMs samples.

ing sliding, so the passive film seems to have a more protective character than in the Al/Al_3Zr system

In terms of friction coefficient, the Al/Al_3Ti FGMs show lower values though they have a higher area fraction of intermetallic platelets and higher hardness values in the outermost regions. The formation of tribolayers anchored on the Al_3Ti fragments, as discussed above, may explain this behaviour.

Regarding the synergism between the wear and corrosion phenomena, Fig. 13 shows the relation between the removed volumes by the mechanical (V_{mech}) and electrochemical (V_{chem}) processes. All the samples show very low values of V_{chem} when compared to V_{mech}. This should be a good indication that the tribocorrosion process is mainly governed by the mechanical wear. It is also observed that the samples having a large V_{mech} show a larger V_{chem}, indicating probably that there exists an increase in the corrosion rate due to wear. Another important characteristic is that the samples with a smaller total wear volume are the 120 *G* ones. This phenomenon can be explained by the higher volume fraction of particles obtained from a higher applied centrifugal force. On the other hand, the 30 *G* and 60 *G* Al/Al_3Ti FGM samples present a smaller total wear volume than the respective Al/Al_3Zr FGMs, probably due to the wear mechanism which does not originate protective tribolayers.

4. Conclusions

In the present work the microstructure and tribocorrosion behaviour of Al/Al_3Ti and Al/Al_3Zr functionally graded materials (FGMs), fabricated by the centrifugal method, was investigated.

It was found that higher applied centrifugal force increases both the intermetallic particles volume fraction as well as their orientation in the outer regions of the FGMs, although the increase of applied centrifugal force from 60 to 120 *G* did not significantly affect the volume fraction or the orientation parameter distribution for the outermost region of the FGMs but did increase it in the adjacent regions. It was observed that Al_3Ti particles have a higher segregation rate with lower applied centrifugal forces than the Al_3Zr particles; a situation that is reversed for higher applied centrifugal forces. Also, higher orientation values for the intermetallic platelets are found in the $Al–Al_3Ti$ FGMs.

Better tribocorrosion behaviour was found in the samples produced with a higher centrifugal force. Considerable differences in the amount of the total wear volume was found between the samples produced at 60 and 120 *G*, regardless the similar volume fraction and orientation parameter of the outermost regions (where the tribocorrosion tests were performed) observed in those samples, indicating that a strong influence of the structure below the surface of the FGM's is determinant in terms of tribocorrosion behaviour. Furthermore, it was observed that the tribocorrosion mechanisms of Al/Al_3Ti and Al/Al_3Zr FGM samples are different, and dependent on the mechanical properties of the reinforcing platelets. The existence of a synergism between the wear and the corrosion is apparent, as higher mechanical wear results in higher relative amount of corrosion.

Acknowledgements

The authors gratefully acknowledge the financial support provided by "Tokai Region Nanotechnology Manufacturing Cluster in KNOWLEDGE CLUSTER INITIATIVE" by the Ministry of Education, Culture, Sports, Science and Technology of Japan. Acknowledgments are also due to "FCT", Portugal, through the project SFRH/BPD/5518/2001.

References

[1] Y.U. Huashun, C. Hongmei, S. Liming, M. Guanghui, Preparation of $Al–Al_3Ti$ in situ composites by direct reaction method, Rare Metals 25 (1) (2006) 32–36.
[2] S.H. Wang, P.W. Kao, The strengthening effect of Al_3Ti in high temperature deformation of $Al–Al_3Ti$ composites, Acta Mater. 46 (8) (1998) 2675–2682.
[3] S.H. Wang, P.W. Kao, C.P. Chang, The strengthening effect of Al_3Ti in ultrafine grained $Al–Al_3Ti$ alloys, Scripta Mater. 40 (3) (1999) 289–295.
[4] Z. Sun, H. Hashimoto, Q. Wang, Y. Park, T. Abe, Synthesis of $Al–Al_3Ti$ composites using pulse discharge sintering process, Mater. Trans. 41 (5) (2000) 597–600.
[5] Y. Fukui, Fundamental investigation of functionally gradient material manufacturing system using centrifugal force, JSME Int. J. Series III 34 (1) (1991) 144–148.
[6] Y. Fukui, Y. Watanabe, Analysis of thermal residual stress in a thick-walled ring of Duralcan-base Al–SiC Functionally graded material, Metal Mater. Trans. A 27A (12) (1996) 4145–4151.
[7] Y. Watanabe, N. Yamanaka, Y. Fukui, Control of composition gradient in a metal–ceramic functionally graded material manufactured by the centrifugal method, Composites Part A 29A (5–6) (1998) 595–601.
[8] Y. Watanabe, Y. Fukui, Fabrication of functionally graded aluminum materials by the centrifugal method, Aluminum Trans. 2 (2000) 195–209.
[9] Y. Watanabe, N. Yamanaka, Y. Fukui, Wear behavior of $Al–Al_3Ti$ composite manufactured by a centrifugal method, Metal Mater. Trans. A 30A (12) (1999) 3253–3261.
[10] Y. Watanabe, H. Sato, Y. Fukui, Wear properties of intermetallic compound reinforced functionally graded materials fabricated by centrifugal solid-particle and in situ methods, J. Solid Mech. Mater. Eng. 2 (7) (2008) 842–853.
[11] L. Lajoye, M. Suéry, Proceedings of International Symposium on Advances in Cast Reinforced Metal Composites, ASM International, 1988, pp. 15–20.
[12] D. Roy, B. Basu, A.B. Mallick, Tribological properties of Ti–aluminide reinforced Al-based in situ metal matrix composite, Intermetallics 13 (7) (2005) 733–740.
[13] J.M. Wu, Z.Z. Li, Contributions of the particulate reinforcement to dry sliding wear resistance of rapidly solidified Al–Ti alloys, Wear 244 (1–2) (2000) 147–153.
[14] D. Landolt, S. Mischler, M. Stemp, Electrochemical methods in tribocorrosion: a critical appraisal, Electrochim. Acta 46 (24–25) (2001) 3913–3929.
[15] P. Jemmely, S. Mischler, D. Landolt, Tribocorrosion behaviour of Fe–17Cr stainless steel in acid and alkaline solutions, Tribol. Int. 32 (6) (1999) 295–303.
[16] P. Jemmely, S. Mischler, D. Landolt, Electrochemical modeling of passivation phenomena in tribocorrosion, Wear 237 (1) (2000) 63–76.

[17] H.C. Brinkman, The viscosity of concentrated suspensions and solutions, J. Chem. Phys. 20 (4) (1952) 571–581.
[18] P.D. Sequeira, Y. Watanabe, H. Eryu, T. Yamamoto, K. Matsuura, Effects of platelet size and mean volume fraction on platelet orientation and volume fraction distributions in functionally graded material fabricated by a centrifugal solid-particle method, Trans. ASME J. Eng. Mater. Technol. 129 (2) (2007) 304–312.
[19] L.F. Mondolfo, Aluminium Alloys: Structure and Properties, Butterworths, London, 1976.
[20] S.H. McGee, R.L. McCullough, Characterization of fiber orientation in short-fiber composites, J. Appl. Phys. 55 (5) (1984) 1394–1403.
[21] L.M. Gonzalez, F.L. Cumbrera, F. Sanchez-Bajo, A. Pajares, Measurement of fiber orientation in short-fiber composites, Acta Metall. Mater. 42 (3) (1994) 689–694.
[22] Y. Watanabe, H. Eryu, K. Matsuura, Evaluation of three-dimensional orientation of Al_3Ti platelet in Al based FGMs fabricated by a centrifugal casting technique, Acta Mater. 49 (5) (2001) 775–783.
[23] A. C. Vieira, P.D. Sequeira, J.R. Gomes, L.A. Rocha Dry sliding wear of Al alloy/SiCp functionally graded composites: influence of processing conditions, Wear, in press. Q1
[24] J.R. Gomes, A.S. Miranda, L.A. Rocha, S.J. Crnkovic, V. Silva, R.F. Silva, Tribological Behaviour of SiC Particulate Reinforced Aluminium Alloy Composites in Unlubricated Sliding Against Cast Iron, Int. J. Appl. Mech. Eng. 7 (2002) 791–802.
[25] S. Mischler, S. Debaud, D. Landolt, Wear-accelerated corrosion of passive metals in tribocorrosion systems, J. Electrochem. Soc. 145 (3) (1998) 750–758.
[26] N. Birbilis, R.G. Buchheit, An experimental survey of electrochemical characteristics for intermetallic phases in aluminum alloys, J. Electrochem. Soc. 152 (4) (2005) 140–151.

Please cite this article in press as: S.C. Ferreira, et al., Microstructural characterization and tribocorrosion behaviour of Al/Al_3Ti and Al/Al_3Zr FGMs, Wear (2011), doi:10.1016/j.wear.2011.02.007